PAPER Special Section on Wide Band Systems

Investigation of Ultra-Wideband Propagation Channel based on a Cluster Scheme

Hiroaki TSUCHIYA[†a)], **Katsuyuki HANEDA**[†], *Student Members*, *and* **Jun-ichi TAKADA**[†], *Member*

SUMMARY In this paper, an Ultra-Wideband (UWB) double-directional channel sounding measurement and spatio-temporal analysis of UWB propagation based on the clusterization approach were reported. After separating the propagation paths and diffuse components both on the transmitter (Tx) antenna and receiver (Rx) antenna positions, the propagation paths both on Tx and Rx positions were observed for clusters separately, while coupling the clusters between Tx and Rx position based on similar time of arrivals, and ray tracing by utilizing high temporal and spatial resolution, respectively. The relation between direction of departure and direction of arrival will then be investigated. For cluster properties, parameters of model characteristics are discussed and compared to other earlier works.

key words: *Ultra Wideband, double directional, UWB channel model, cluster*

1. Introduction

Ultra-Wideband (UWB) radio systems are currently receiving a great deal of attention for the future of short-range wireless communication due to its ultra high data rate and low power transmission [1], [2]. UWB signals are defined as having a −10 dB bandwidth of at least 500 MHz or a −10 dB fractional bandwidth greater than 20%. So its signals are radiated by the transmitter (Tx) antenna with very short pulses. These short pulses allow a receiver to precisely distinguish or resolve the different multipath components which come from different directions and with different delay times arriving at the receiver (Rx) antenna. The power of these multipath components is often effectively combined by using a rake receiver architecture. However, some dense multipath components often cause waveform distortion if the pulses are ambiguous. UWB system performance suffers from this problem.

Antennas also affect the performance of UWB systems. In narrowband systems, the channel model is often considered including antenna elements because their characteristics are essentially flat over small bandwidths. However, in UWB systems, the frequency characteristics of antennas cannot be disregarded and they will cause a dramatic distortion of the waveform within each of the individual paths. Therefore, to separate the antenna effects from the channel model, not only the time of arrival (TOA) of each path is important, but the direction of departure (DOD) and direction of arrival (DOA) are also necessary because they enable us to remove the antenna characteristics from each path if the Tx and Rx antenna characteristics are provided. This is proposed in the double-directional channel of [3]. For extending to UWB propagation model, it is contended that TOA and DOD/DOA of each path are constant over the bandwidth, but the complex frequency spectrum of the path should be considered [4]. This model is independent of antennas and is useful to evaluate the antenna effects when designing UWB systems. In our earlier works, we have already discussed the estimation of multipath parameters using the successive interference cancellation (SIC) [5] space-alternating generalized expectation maximization (SAGE) algorithm [6]–[8] based on maximum likelihood (ML). The algorithm is used to estimate wideband channel parameters and spectrum of each path, but the cluster properties were not analyzed. In this paper, we present the results of UWB double-directional propagation measurement in an office environment using a composition array, where the paths are determined by using SIC-SAGE. We focus on the detailed analysis of the clusters and compare it with earlier works.

2. Measurement Setup

The measurements have been performed in the frequency domain with a vector network analyzer (VNA) to determine the complex radio channel transfer function $H(f) = S_{21}(f)$. Some indispensable parameters are shown in Table 1. The measured frequency bandwidth implies a delay time resolution of 0.13 ns. The spectrum was divided into 751 frequency sweeping points, resulting in 10 MHz between frequency samples and a maximum delay time of 100 ns. The antenna elements spacing is fixed at 48 mm which corresponds to $\lambda/2$ at the lowest frequency.

Figures 1(a) and 1(b) show the DOD measurement and DOA measurement of the UWB double-directional channel sounding system respectively. First, the Rx antenna was mounted on a pole and its position was fixed at the center of the Rx array. While the Tx antenna was mounted on the arm of the X-Y-Z scanner to measure the DOD. After the scanning of Tx was finished, we scanned the opposite side to measure the DOA, while fixing Tx at the center of the Tx array. All processes were controlled automatically by GPIB, as well as the data acquisition. We conducted 700 spatial samples of multiple-input-single-output/single-input-multiple-output (MISO/SIMO) measurements, so that

Manuscript received March 3, 2006.
Manuscript revised May 20, 2006.
Final manuscript received July 18, 2006.

[†]The authors are with the Department of International Development Engineering, Graduate School of Science and Engineering, Tokyo Institute of Technology, Tokyo, 152-8550 Japan.
a) E-mail: tutiya@ap.ide.titech.ac.jp

DOI: 10.1093/ietfec/e89–a.11.3095

Table 1 Specifications of the experiment.

Bandwidth	3.10 to 10.60 GHz [9]
Frequency sweeping points	751
Spatial sampling in the Rx and Tx position	$10 \times 10 \times 7$ points in X-Y-Z with element spacing of 48 mm (less than half wavelength at 3.1 GHz)
Estimated parameters	DOD and DOA azimuth, elevation angle, delay time, spectrum, and curvature radius
Type of antennas	Biconical [10]
Polarization	Vertical-Vertical
Calibration	Function of VNA and back-to-back (1 m)
IF bandwidth of VNA	100 Hz
SNR at receiver	30 dB
Snapshot	1

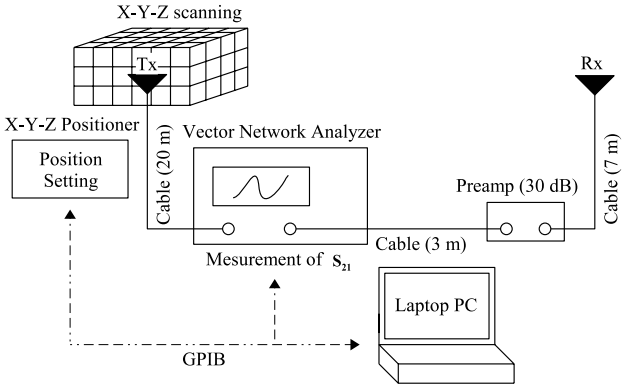

(a) DOD measurement (MISO)

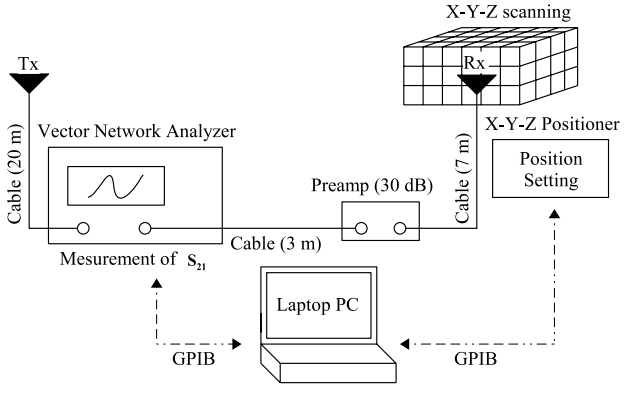

(b) DOA measurement (SIMO)

Fig. 1 UWB double-directional channel sounding system.

the maximum size of the array implies the Fourier azimuthal angular resolution of 10.0 deg. Since the spherical wave array mode vector can better model the path for short range environments compared to the plane wave model [11], it was adopted through out the paper. However the spherical wave model cannot be applied to simultaneous DOD-DOA estimation since it assumes either a point source or a point observer in Tx or Rx position respectively, and different radiant point sources in the Tx array result in the complex combination of spherical waves approaching the Rx array [11]. Thus we estimated DODs and DOAs separately by using two single directional channel setups (MISO/SIMO) instead of MIMO to avoid this conflict, then combine them with TOA and ray tracing.

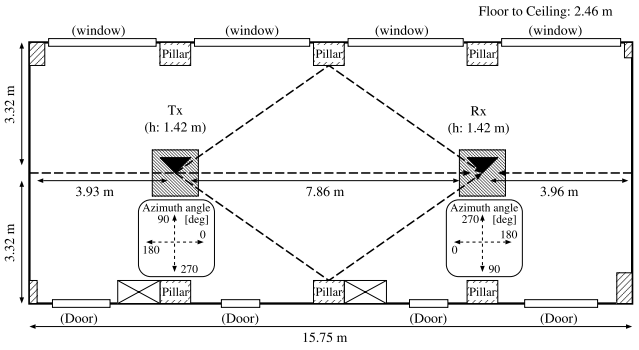

(a) Top view

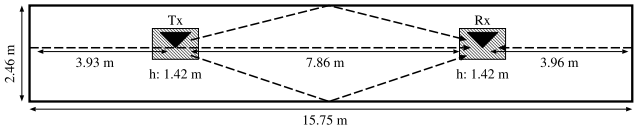

(b) Side view

Fig. 2 The experiment environment.

3. Measurement Environment

The measurement was performed in an empty office room, with no furniture. Figure 2 shows the top and side view of the room. Note that the azimuth angle is defined with respect to the line-of-sight (LOS), and is opposite for the Tx and Rx positions. The room has a floor area of 15.75×6.64 m and a height of 2.46 m. The center height of the array is 1.42 m from floor for both at Tx and Rx positions, and the distance of LOS is 7.86 m. There are 4 metal doors and 4 windows with metal frames. The walls consists mostly of reinforced concrete and 10 pillars are uniformly distributed around the room.

4. Data Processing and Analysis

From the measurement data, the parameters and spectrum of each path were modeled as follows:

$$y(f, \phi_{tx}, \theta_{tx}, \phi_{rx}, \theta_{rx}, \tau) = D_{tx}(f, \phi_{tx}, \theta_{tx}) a(f, \tau) r(f) D_{rx}(f, \phi_{rx}, \theta_{rx}) \quad (1)$$

where

- $y(f, \phi_{tx}, \theta_{tx}, \phi_{rx}, \theta_{rx}, \tau)$: the transfer function of each path,
- f : the frequency,
- ϕ_{tx}, θ_{tx} : azimuth and elevation angles of DOD,
- ϕ_{rx}, θ_{rx} : azimuth and elevation angles of DOA,
- τ : delay time,
- $a(f, \tau)$: complex gain of the spatial propagation,
- $r(f)$: scattering loss,
- $D_{tx}(f, \phi_{tx}, \theta_{tx})$: radiation pattern of Tx antenna for a single polarization.

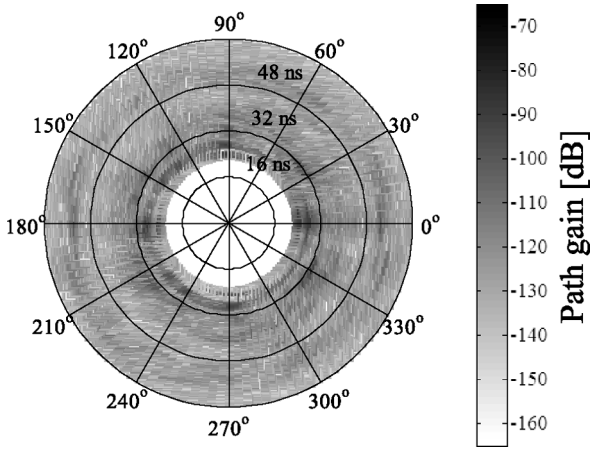

(a) Total power spectrum

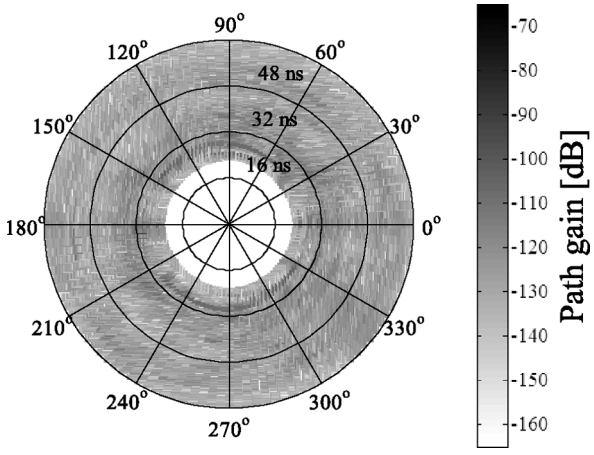

(b) Residual spectrum after the extraction of 120 paths

Fig. 3 Azimuth - delay power spectrum at Tx.

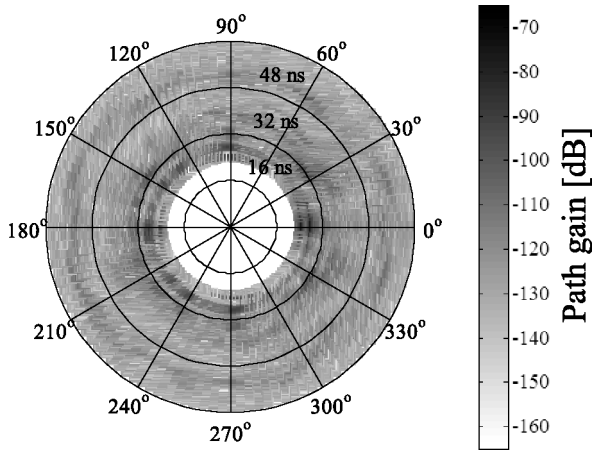

(a) Total power spectrum

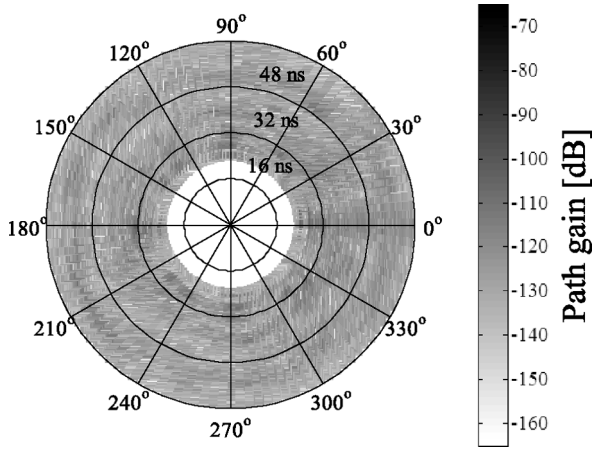

(b) Residual spectrum after the extraction of 120 paths

Fig. 4 Azimuth - delay power spectrum at Rx.

- $D_{rx}(f, \phi_{rx}, \theta_{rx})$: radiation pattern of Rx antenna for a single polarization.

The model parameters are estimated using the SAGE algorithm implemented with SIC process, a simplified ML based estimator. Details of the algorithm are presented in [8], [11].

4.1 Separation of Propagation Paths and Diffuse Components

Figures 3(a) and 4(a) show the azimuth-delay power spectrum at Tx and Rx respectively. These figures are constructed by using inverse Fourier transform and beamforming to estimate TOAs and DODs/DOAs respectively. The LOS appears near position $(\tau, \phi) = (27\,\text{ns}, 0\,\text{deg})$, and also its sidelobe appears between delay time $\tau = 25\,\text{ns}$ to $\tau = 30\,\text{ns}$ at all azimuth angles. To separate the propagation paths and diffuse components, we should calculate the noise floor. The noise floor level of the VNA was -100 to $-90\,\text{dB}$. The noise level in Figs. 3 and 4 are reduced to -150 to $-140\,\text{dB}$, after inverse Fourier transform and beamforming of the data for 700 elements of the array and 751 frequency sweeping points. The amount of the noise reduction is estimated as $10\log_{10}(700 \times 751) \simeq 57\,\text{dB}$. We detected 120 paths at each Tx and Rx positions, while the residuals were considered as diffuse components shown in Figs. 3(b) and 4(b). It still seems to have several undetected paths which are shown in Figs. 3(b) and 4(b), but the noise floor level makes it difficult to continue to detect paths by using the SAGE algorithm. The power of specular paths which are detected both at Tx and Rx positions consists of about 70% of the total power. The total power is defined as the sum of all squared measured data, and is $-68.35\,\text{dB}$ and $-68.45\,\text{dB}$ at Tx and Rx positions respectively. As shown in [12], [13], the power of specular paths consisted of about 70% and 90% of the total power respectively by using the same algorithm.

4.2 Clusterization of Propagation Paths

Figures 5 and 6 show the detected propagation paths in angular-delay domains at Tx and Rx positions respectively. These results show that the detected paths tend to form some clusters in the angular-delay domain. We define a cluster as an accumulation of detected paths with similar TOAs and DODs for the Tx position and similar TOAs and DOAs for the Rx position [14]. Moreover, the clusters are related to the physical structures of the measured environment i.e.,

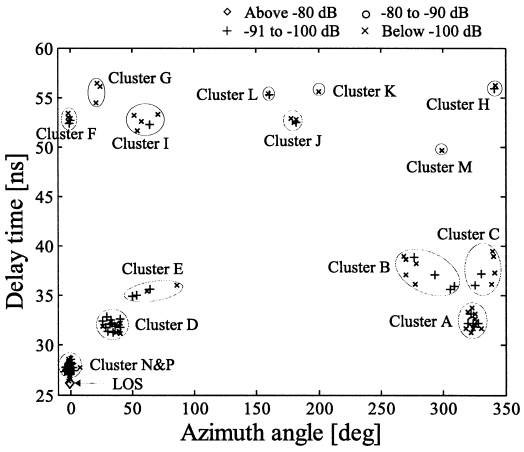

Fig. 5 Clusterization of propagation paths at Tx.

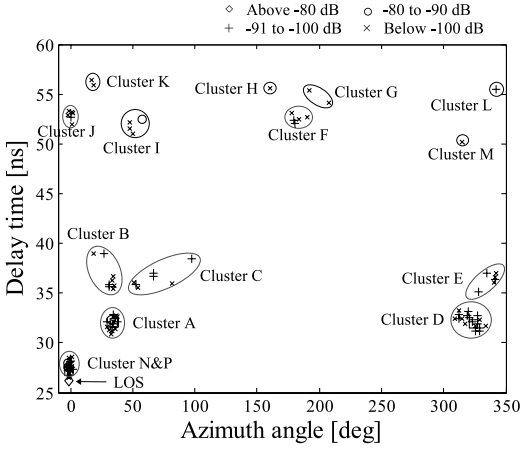

Fig. 6 Clusterization of propagation paths at Rx.

specular reflection path, material, position and size of reflection objects, using a heuristic approach.

4.3 Coupling the Clusters between the Tx and Rx Positions and Antenna Deconvolution

The clusters were coupled between the Tx and Rx position based on delay time and ray tracing. The ray tracing is used for coupling the clusters based on delay time when the specular path is detected. We then see that all clusters can be coupled and thus are given the same name on both sides. The identification of these clusters are also shown in Figs. 5, 6 and 7. Their positions in the real environment are shown in Fig. 8.

Two kinds of clusters are identified considering the relation between the Tx and Rx positions. One is the single bounce clusters i.e., Clusters A, B, C, D, E, F, J, N and P, which at both Tx and Rx positions have close TOA and DOD/DOA of same scatterers which are identified by using ray tracing. The others are the multi-bounce clusters i.e., Clusters G, H, I, K, L and M, which at both Tx and Rx positions have close TOA but DOA and DOD are from different scatterers. Because all of these clusters have long delay times, these paths are not scattered by a single object. The multi-bounce clusters also have close relation in the DODs and DOAs by using ray tracing. Note that the relation of these clusters can only be investigated by using double-directional channel measurements. The detailed identification of reflection objects are shown in Table 2 and Fig. 7. After coupling the clusters, the antenna deconvolution is done. The antenna gains both at Tx and Rx were removed from the detected paths in the frequency and angular domains. This is the advantage of the double-directional measurement which gives the DOD and DOA.

Table 2 Reflection objects of clusters.

Cluster	Reflection objects		
A	pillar	H	wall & pillar
B	door	I	door & window frames
C	door & wall	J	wall
D	pillar	K	wall & door
E	pillar	L	wall & pillar
F	wall	M	door & pillar
G	wall & window frames	N	ceiling
		P	floor

5. Cluster Properties

For the inter cluster properties, it is hard to mention the relationship among clusters since the number of measurement data are not large enough to conclude it. For the intra-cluster properties, the probability density function (pdf) and power spectrum density (PSD) both dependent on delay time and azimuth angle are shown in Figs. 9–12. In papers [15]–[19], the clustering of multipath components were reported for delay or both delay and angular domains. In these papers, the inter cluster path decay rate and the intra-cluster path decay rate are shown, and related with the double exponential decay law. Based upon these models, we show the intra-cluster properties, and try to compare with their results.

5.1 Pdf of Intra-Cluster

Figures 9 and 10 show the intra-cluster pdfs of delay time and angular domains respectively. Figure 9 is constructed by normalizing the delay time of the intra-cluster paths to the delay time of the path with highest power within each cluster. For Fig. 10, the angle of the path with the highest power is used for the normalization. The delay times are distributed as a best fit exponential pdf which is given as follows [15]:

$$p(\tau_{k,l} \mid \tau_{k-1,l}) = \alpha e^{-\alpha(\tau_{k,l}-\tau_{k-1,l})} \tag{2}$$

where α is the intra-cluster path generation rate, and $\tau_{k,l}$ is the delay time of the kth arrival path in the lth cluster. Note that, $1/\alpha$ is called the intra-cluster path decay rate, and at the same time it is equivalent to the standard deviation of relative delay time. For the distribution of azimuth angles, it is shown as a best fit Laplacian pdf which is given as follows:

$$p(\phi_{k,l}) = \frac{1}{\sqrt{2}\sigma} e^{-|\sqrt{2}\phi_{k,l}/\sigma|} \tag{3}$$

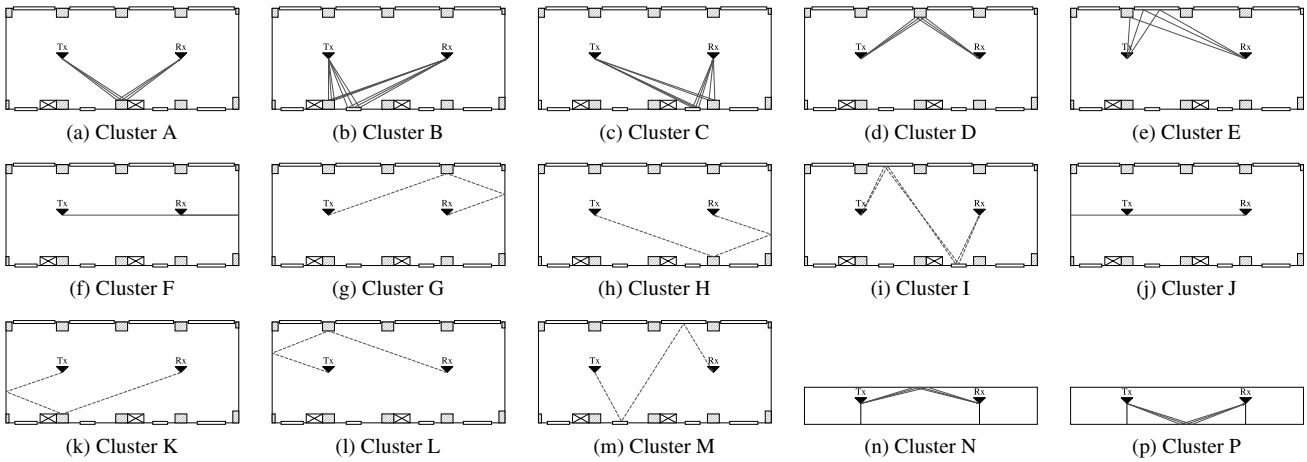

Fig. 7 Identification of clusters.

Fig. 8 Cluster identification in the real environment.

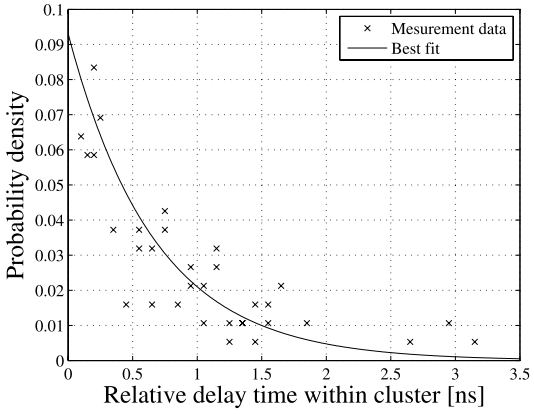

Fig. 9 Delay pdf of intra-clusters.

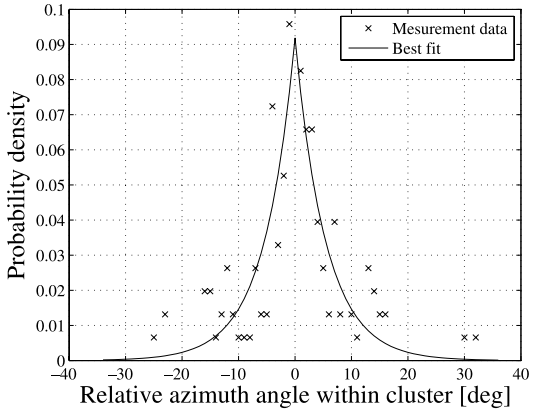

Fig. 10 Angular pdf of intra-clusters.

where $\phi_{k,l}$ is the relative angle with respect to the cluster center, and σ is the standard deviation of relative angles. For the conditional joint pdf of delay time and angle, it can be given as follows:

$$p(\tau_{k,l}, \phi_{k,l} \mid \tau_{k-1,l}) = p(\tau_{k,l} \mid \tau_{k-1,l}) \cdot p(\phi_{k,l}). \quad (4)$$

From (4), the unconditional joint pdf can be re-expressed as follows [14]:

$$p(\tau_{k,l}, \phi_{k,l}) = p(\tau_{k,l}) \cdot p(\phi_{k,l}). \quad (5)$$

5.2 PSD of Intra-Cluster

Figures 11 and 12 show the PSD of delay time and angle. These figures are also constructed by normalizing the delay/angle of the intra-cluster paths to the delay/angle of the

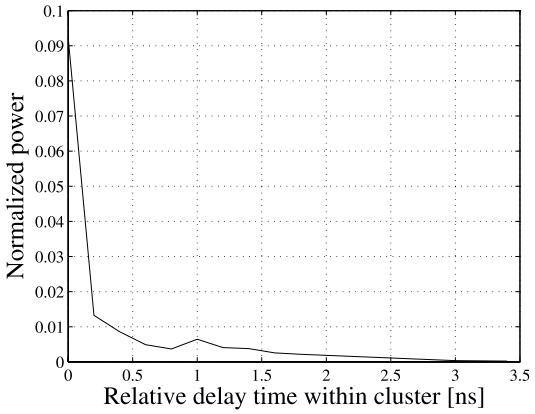

Fig. 11 Delay-power spectrum density of intra-clusters at 0.20 ns resolution.

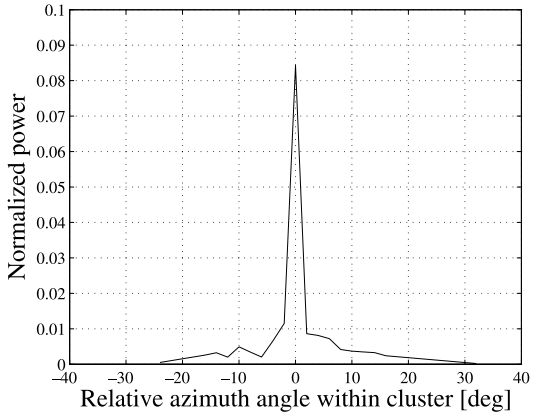

Fig. 12 Angular-power spectrum density of intra-clusters at 2.0 deg resolution.

path with highest power within each cluster. And furthermore, the normalized power of each delay/angle are multiplied by its corresponding pdf. It is hard to plot a best fit of these distributions, because the number of measurement data are not large enough to conclude them. The PSD of delay time is defined as follows:

$$P(\tau_{k,l}) = E\left\{| h(\tau_{k,l}) |^2\right\} \tag{6}$$

where $E\{\cdot\}$, $|\cdot|$ and $h(\tau_{k,l})$ are the expected value, the absolute value and delay impulse response of the intra-cluster path, respectively. For the PSD of angle, it is defined as follows:

$$P(\phi_{k,l}) = E\left\{| h(\phi_{k,l}) |^2\right\} \tag{7}$$

where $h(\phi_{k,l})$ is the angular impulse response intra-cluster path. From (6) and (7), the joint PSD of delay time and angle can be expressed as follows:

$$P(\tau_{k,l}, \phi_{k,l}) = E\left\{| h(\tau_{k,l}, \phi_{k,l}) |^2\right\} = P(\tau_{k,l}) \cdot P(\phi_{k,l}) \tag{8}$$

where $h(\tau_{k,l}, \phi_{k,l})$ [16] is the combined impulse response of the intra-cluster path. The powers of the highest path within each cluster follows the inter cluster path decay rate [15]–[17], and the power of other paths within each cluster can be related to a joint PSD which is easily expressed as follows [20]:

$$P(\tau_{k,l}, \phi_{k,l}) \propto E\left\{| \beta_{k,l} |^2 | \tau_{k,l}, \phi_{k,l}\right\} \cdot p(\tau_{k,l}, \phi_{k,l}) \tag{9}$$

where $\beta_{k,l}$ [17] is the amplitude of the intra-cluster paths, and $E\left\{|\beta_{k,l}|^2|\tau_{k,l}, \phi_{k,l}\right\}$ is the expected power of the intra-cluster path conditioned on their delay times and angles. The notation $A \propto B$ means that the two terms A and B are proportional.

5.3 Comparison with Earlier Works

The intra-cluster standard deviation of relative delay time determined by UWB propagation measurement was shorter than that reported in [15]–[17]. A standard deviation of relative delay time of $1/\alpha$=0.65 ns was obtained for the best fit exponential distribution for the relative delay times of path arrivals (2), while the standard deviations of $1/\alpha$=2.30 ns, $1/\alpha$=5.00 ns, $1/\alpha$=5.10 ns and $1/\alpha$=6.60 ns were reported in [15]–[17].

The standard deviation of relative angles was smaller than those reported in [15]–[17]. A relative angular standard deviation of σ=8.4 deg was obtained for the best fit Laplacian distribution for the relative angles of path arrivals (3), while values of σ=21.5 deg, σ=25.5 deg and σ=37.0 deg were reported in [16], [17].

Possible reasons for shorter delay and smaller angular standard deviations might depend on the building architecture. For example, smaller room size will lead to a shorter decay and smaller angular standard deviation. Another reason is that the time resolutions of the post-processing algorithms were different. The fractional bandwidth should also be considered. The time and angular resolutions of the experiment are 0.13 ns and 10.0 deg respectively, and these values are finer than the ones reported in [16], [17]. The parameters of the UWB propagation modeling compared with earlier works in [15]–[17] are shown in Table 3.

6. Conclusion

In this paper, a 3-D double-directional UWB channel measurement and modeling based on the clusterization approach was reported. DODs and DOAs were estimated separately, and were related by using high resolution TOAs and ray tracing. Double-directional channel models are prerequisites for deconvolving the Tx and Rx antenna transfer functions and constructing the propagation model that is independent of the antenna. Most of the clusters were determined by physical structures of the experiment environment. Intra-cluster properties were derived in the delay and angular domains, with their pdf distributions found to be modeled by exponential and Laplacian functions respectively. The propagation model parameters both of relative delay times and relative angles within clusters are shown, and their PSD distributions are also derived from the measurement data. With these information, the channel can be easily reproduced.

Table 3 Comparison of channel models.

Parameter	UWB (this paper)	UWB [17]	Clyde Building [16]	Crabtree Building [16]	Saleh-Valebzuela [15]
Environment [m]	15.7×6.6	6.6×5.1	-	-	115.0×14.0
Bandwidth [GHz]	3.10 to 10.60	3.10 to 10.60	6.75 to 7.25	6.75 to 7.25	1.40 to 1.60
Time resolution [ns]	0.13	1.00	3.00	3.00	10.00
Angular resolution [deg]	10.0	10.0	6.0	6.0	-
Estimation method	SAGE	CLEAN	CLEAN	CLEAN	-
$1/\alpha$ [ns]	0.65	2.30	5.10	6.60	5.00
σ [deg]	8.4	37.0	25.5	21.5	-

The parameters of pdfs are smaller than earlier works in [15]–[17] due to the smaller building architecture and time resolutions of post-processing algorithms. This means it is not conclusive to say which model in [15]–[17] can be a general model representation for many different types of buildings and rooms, because UWB signals have strong frequency dependent effects. It will be determined by reflection objects and affected by the real environment. One also can say from this report that not only the statistical channel model is important but also the deterministic channel model is necessary.

Acknowledgment

The authors would like to thank Mr. Kriangsak Sivasondhivat and Mr. Gilbert Siy Ching from Tokyo Institute of Technology for the helpful discussions and proofreading of this paper.

References

[1] R. Kohno, "Overview of UWB systems—Trends of R & D and regulation," 2003 Microwave Workshop & Exhibition (MWE2003) Digest, Nov. 2003.
[2] T. Kobayashi, F. Ohkubo, N. Takahashi, M. Yoshikawa, T. Miyamoto, H. Zhang, J. Takada, and K. Araki, "Overview and trends of UWB (ultra wideband) propagation studies," IEICE Technical Report, WBS2003-1, May 2003.
[3] M. Steinbauer, A.F. Molisch, and E. Bonek, "The double-directional radio channel," IEEE Antennas Propag. Mag., vol.43, no.4, pp.51–63, Aug. 2001.
[4] K. Haneda, J. Takada, and T. Kobayashi, "Double directional ultra wideband channel characterization in a line-of-sight home environment," IEICE Trans. Fundamentals, vol.E88-A, no.9, pp.2264–2271, Sept. 2005.
[5] B.H. Fleury, X. Yin, K.G. Rohbrandt, P. Jourdan, and A. Stucki, "Performance of a high-resolution scheme for joint estimation of delay and bidirection dispersion in the radio channel," Proc. IEEE 55th Veh. Technol. Conf., pp.522–526, May 2002.
[6] J.A. Fessler and A.O. Hero, "Space-alternating generalized expectation maximization algorithm," IEEE Trans. Signal Process., vol.42, no.10, pp.2664–2677, Oct. 1994.
[7] B.H. Fleury, M. Tschudin, R. Heddergott, D. Dahlhaus, and K.I. Pedersen, "Channel parameter estimation in mobile radio environments using the SAGE algorithm," IEEE J. Sel. Areas Commun., vol.17, no.3, pp.434–449, March 1999.
[8] J. Takada, K. Haneda, and H. Tsuchiya, "Joint DOA/DOD/DTOA estimation system for UWB double directional channel modeling," in Advances in Direction of Arrival Estimation, ed. S. Chandran, Artech House, Norwood, MA, USA, 2006.
[9] Federal Communications Commission, "Revision of part 15 of the commission's rules regarding ultra-wideband transmission systems," First Report and Order, FCC 02–48, April 2002.
[10] S. Promwong, W. Hachitani, and J. Takada, "Free space like budget evaluation of UWB-IR system," Proc. 2004 International Workshop on Ultra Wideband Systems Joint with Conference on Ultra Wideband Systems and Technologies (UWBST & IWUWBS2004), pp.312–316, Kyoto, Japan, May 2004.
[11] K. Haneda, J. Takada, and T. Kobayashi, "A parametric UWB propagation channel estimation and its performance validation in an anechoic chamber," IEEE Trans. Microw. Theory Tech., vol.54, no.4, pp.1802–1811, 2006.
[12] K. Haneda, J. Takada, and T. Kobayashi, "Clusterization analysis of spatio-temporal UWB radio channel for line-of-sight and non-line-of-sight indoor home environment," Joint COST273/284Workshop and COST273 10th MCM, Gothenburg, Sweden.
[13] H. Tsuchiya, K. Haneda, and J. Takada, "Reflection and scattering analysis of Ultra Wideband indoor propagation measurements," Technical Meeting on Instrumerntation and Measurement, IEE Japan, IM-04-20, June 2004.
[14] C.C. Chong, C.M. Tan, D.I. Laurenson, S. McLaughlin, M.A. Beach, and A.R. Nix, "A new statistical wideband spatio-temporal channel model for 5-GHz band WLAN systems," IEEE J. Sel. Areas Commun., vol.21, no.2, pp.139–150, Feb. 2003.
[15] A.A.M. Saleh and R.A. Valenzuela, "A statistical model for indoor multipath propagation," IEEE J. Sel. Areas Commun., vol.SAC-5, pp.128–137, Feb. 1987.
[16] Q. Spencer, B. Jeffs, M. Jensen, and A. Swindlehurst, "Modeling the statistical time and angle of arrival characteristics of an indoor multipath channel," IEEE J. Sel. Areas Commun., vol.18, no.3, pp.347–360, March 2000.
[17] R.J.-M. Cramer and R.A. Scholtz, "Evaluation of an ultra-wide-band propagation channel," IEEE Trans. Antennans Propag., vol.50, no.5, pp.561–570, May 2002.
[18] H. Hashemi, "The indoor radio propagation channel," Proc. IEEE, vol.81, pp.943–968, July 1993.
[19] Q. Spencer, M. Rice, B. Jeffs, and M. Jensen, "A statistical model for the angle-of-arrival in indoor multipath propagation," Proc. IEEE Veh. Technol. Conf., pp.1415–1419, 1997.
[20] K.I. Pedersen, P.E. Mogensen, and B.H. Fleury, "A stochastic model of the temporal and azimuthal dispersion seen at the base station in outdoor propagation environments," IEEE Trans. Veh. Technol., vol.49, no.2, pp.437–447, March 2000.

Hiroaki Tsuchiya received the B.E. degree from Tokyo University of Agriculture and Technology, Japan, in 2003, and M.E. degree from Tokyo Institute of Technology, Japan, in 2005. At present, he is studying towards a Ph.D. degree at Tokyo Institute of Technology. His research interests focus on the wireless propagation channel characterization and modeling of ultra wideband radio.

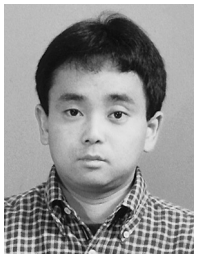

Katsuyuki Haneda received the B.E. and M.E. degrees from the Tokyo Institute of Technology, Tokyo, Japan, in 2002 and 2004, respectively. His current interests are radio propagation measurements and modeling, array signal processing, UWB radio, and multiple-input multiple-output systems. He is currently a Research Fellow with the Japan Society for the Promotion of Science, Tokyo, Japan. Mr. Haneda was the recipient of the Student Paper Award presented at the 7th International Symposium on Wireless Personal Multimedia Communications (WPMC'04).

Jun-ichi Takada received the B.E., M.E., and D.E. degrees from the Tokyo Institute of Technology, Tokyo, Japan, in 1987, 1989, and 1992, respectively. From 1992 to 1994, he was a Research Associate Professor with Chiba University, Chiba, Japan. From 1994 to 2006, he was an Associate Professor with Tokyo Institute of Technology. Since 2006, he has been a Professor with Tokyo Institute of Technology. His current interests are wireless propagation and channel modeling, array signal processing, UWB radio, cognitive radio, applied radio instrumentation and measurements, and ICT for international development. Dr. Takada is a member of IEEE, ACES, and the ECTI Association Thailand.